Photoinduced Solvent Ligation to Nickel(II) Octaethylporphyrin Probed by Picosecond Time-Resolved Resonance Raman Spectroscopy

Yuki Uesugi,[†] Yasuhisa Mizutani,[†,‡] and Teizo Kitagawa*[,†,‡]

School of Mathematical and Physical Science, The Graduate University for Advanced Studies and Institute for Molecular Science, Okazaki National Research Institutes, Myodaiji, Okazaki 444, Japan

Received: February 24, 1998; In Final Form: April 27, 1998

Pump/probe picosecond time-resolved resonance Raman spectra of nickel(II) octaethylporphyrin (NiOEP) in pyridine were observed in the time range −5 to +1000 ps. The spectra demonstrate generation of the vibrationally and electronically excited (d,d) state (B_{1g}) immediately after the excitation to the $\pi\pi^*$ state of the macrocycle, subsequent vibrational relaxation, and the formation of six-coordinate exciplex, $B_{1g}(L)_2$ (L = pyridine). Singular value decomposition analysis was applied to a series of picosecond time-resolved Raman spectra to investigate whether a five-coordinate complex was generated prior to the formation of the six-coordinate species. The results indicate insignificant population of the five-coordinate species preceding the formation of $B_{1g}(L)_2$ and suggest concerted coordination of two solvent molecules to axial positions of the (d,d) excited NiOEP. The formation process of the $B_{1g}(L)_2$ species is discussed.

Introduction

Nickel(II) octaethylporphyrin (NiOEP) has been extensively studied to elucidate basic physicochemical properties of metalloporphyrins. The electronic configuration of the Ni(II) atom in the ground state of NiOEP is $(d_{xy})^2(d_{xz})^2(d_{yz})^2(d_{z^2})^2$ with A_{1g} symmetry but the lowest excited state of the metal (B_{1g}), obtained by promotion of an electron from the filled d_{z^2} to an empty $d_{x^2-y^2}$ orbital, lies considerably below the lowest excited $\pi\pi^*$ state (E_u) of the macrocycle.[1] This metal B_{1g} state plays a key role in the photophysical behaviors of NiOEP. The excited-state dynamics of NiOEP have been investigated by picosecond and femtosecond transient absorption spectroscopy[2−6] and resonance Raman (RR) and resonance coherent anti-Stokes Raman scattering, both in the time-resolved[7−9] and saturation regimes.[10−12] Vibrational relaxation of NiOEP in the (d,d) excited state in noncoordinating solvents has also been explored with picosecond time-resolved RR (ps-TR^3) spectroscopy.[13]

Theoretical calculations have shown that the lowest excited (d,d) state of the metal (B_{1g}) of NiOEP in noncoordinating solvents lies at only 3000 cm^{-1} above the A_{1g} state.[1] Photoexcitation of NiOEP to the E_u state of porphyrin in toluene and tetrahydrofuran (THF) results in ultrafast radiationless relaxation to the (d,d) excited state within 350 fs,[5] from which the molecule relaxes to the ground electronic state with a time constant of ca. 250 ps. In a weakly coordinating solvent such as pyridine, however, it is possible that two pyridine molecules coordinate to axial positions of Ni in the (d,d) excited state, forming a six-coordinate species, $B_{1g}(L)_2$ (L = pyridine),[4] while its ground electronic state prefers the same four-coordinate structure observed for the complex in a noncoordinating solvent such as toluene. Recent femtosecond transient absorption experiments suggest that photoassociation/dissociation of solvent molecules to/from NiOEP takes place in various organic solvents[14] but that such coordination changes and the possible coexistence of the five- and six-coordinate species remain to be clarified by a more direct method such as vibrational spectroscopy.

Three molecular structures with various degrees of planarity have been identified by X-ray crystallographic analyses for two crystalline forms of NiOEP.[15,16] For the planar form of the ground-state NiOEP in noncoordinating solvents, static RR and infrared (IR) spectra have been thoroughly analyzed on the basis of the observations of isotopic frequency shifts and normal-coordinate calculations.[17,18] Effects of nonplanar distortions of the macrocycle[19,20] and changes of the metal spin state[21] have also been discussed from static RR spectra. Accordingly, in this study, we have investigated the transient RR spectra of NiOEP in pyridine with ps-TR^3 spectroscopy with the light sources reported previously.[22] Singular value decomposition (SVD) analysis has been used to identify a number of spectral intermediates involved in photochemical processes of bacteriorhodopsin,[23−26] retinals,[27] and other molecules.[28−31] The series of ps-TR^3 spectra observed were analyzed with the SVD method both in time and frequency domains. The photodynamical processes of NiOEP in pyridine will be discussed.

Experimental and Analysis

Setup for ps-TR^3 Measurements. The block diagram of apparatus for ps-TR^3 measurements is illustrated in Figure 1. The second harmonic (385−415 nm) of the output from a picosecond titanium:sapphire laser (Spectra Physics, Tsunami) amplified by a regenerative amplifier (Positive Light, Spitfire) at 1 kHz was generated by a β-barium borate crystal (BBO1). The temporal width of a pulse was ca. 2.5 ps at this stage. In the system shown in Figure 1a, the second harmonic was separated from the fundamental by a dichroic mirror (DM). The second harmonic was used as a probe pulse for pump/probe time-resolved resonance Raman measurements, and the fundamental was focused into heavy water in a 10 cm long cylindrical cell to generate white light continuum (WLG). Optical parametric amplification (OPA) was performed by mixing the white light continuum with a part of the second harmonic in a 7 mm

* To whom correspondence should be addressed.
† The Graduate University for Advanced Studies.
‡ Institute for Molecular Science.

S1089-5639(98)01277-8 CCC: $15.00
Published on Web 06/23/1998

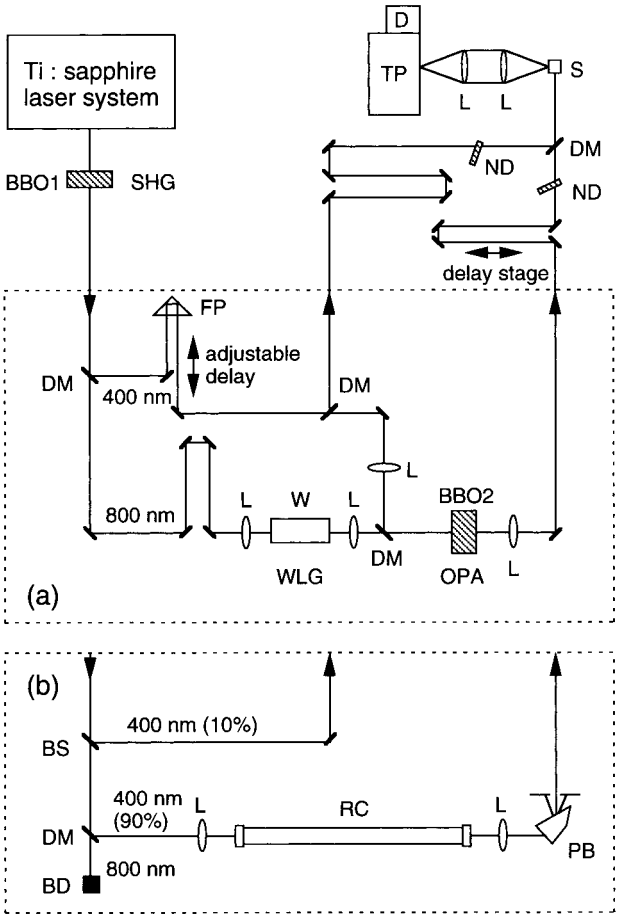

Figure 1. Schematic diagram of the ps-TR^3 measurement system constructed in this study: (a) pumping by the output of the WLG/OPA system; (b) pumping by stimulated Raman scattering. W, water in a 10-cm long cylindrical cell; DM, dichroic mirrors; BS, beam splitter; BD, beam dumper; L, focusing lenses; FP, 180° folding prism; RC, 1 m long Raman shifting cell filled by high-pressure H_2 gas; PB, Pellin-Broca prism; ND, variable neutral density filter; S, sample; TP, triple polychromator; D; photodiode array detector.

thick BBO crystal (BBO2). Details of the WLG/OPA system and the nature of the generated light pulses were described previously.[22]

In the other system shown in Figure 1b, the second harmonic was split into two parts by a 10% reflective beam splitter (BS). The reflected second harmonic (10%) was used as a probe pulse of Raman scattering with the remaining portion (90%) used to excite stimulated Raman scattering of high-pressure (50 kg/cm^2) H_2 gas contained in a 1 m long cell. The first Stokes component of the stimulated Raman scattering was used as a pump pulse to initiate the photoreaction of NiOEP. The energy of the pump and probe pulses were adjusted to 13−15 and 1.5−2.0 mJ/pulse, respectively, with neutral density (ND) filters. The pump and probe pulses were combined collinearly and line-focused with lenses on the sample solution in a 10 × 10 × 50 mm^3 quartz cell. The timing of the illumination by the pump and probe pulses was adjusted by the adjustable optical delay stage consisting of two mirrors, operated by stepping motors. The point of 0 ps delay between the pump and probe pulses was determined by the rise of transient absorption due to the formation of the S_1 state of rhodamine 6G. The instrument response function of this system was also determined with the rise of transient absorption of the S_1 rhodamine 6G.

The solution in the sample cell was continuously stirred by a magnetic stirrer during the measurement to protect the sample from damages by the repeated illumination of intense pump pulses. Raman scattered light in backscattering geometry was collected, collimated by a lens, and focused onto the entrance slit of a triple polychromator (Spex 1877) by another lens. The dispersed light was detected with an intensified photodiode array (EG & G PARC, model 1421) that has 1024 active pixels (25 mm × 25 μm/pixel). The detected signals were A/D converted and transferred to a personal computer.

The ground-state absorption spectra of NiOEP in piperidine/toluene mixed solvents were measured by the following method: a toluene solution of NiOEP was prepared and divided into two portions. A volume of one portion was determined precisely before complete evaporation of the solvent. Exactly the same volume of piperidine was then added to the vessel. This solution was mixed with the other portion of the solution in various ratios, and absorption spectra were measured with a spectrophotometer (Hitachi, U-3210). NiOEP (Aldrich), spectroscopic grade pyridine (Dojindo Laboratories) and toluene (Dojindo Laboratories), and piperidine (Wako Pure Chemicals) were used without further purification.

Singular Value Decomposition Analysis for Time-Resolved Spectra. The computer program for SVD analysis was coded on the basis of the algorithm described in ref 32. Time-resolved spectral data are arranged in a $m \times n$ matrix, **A**, in which m and n correspond to the numbers of delay time points and wavenumber points, respectively. In this study m is 99 and n is 900. Matrix **A** is converted to an $n \times n$ diagonal matrix, **W**, by means of an $m \times n$ orthogonal matrix, **U**, and an $n \times n$ orthogonal matrix, **V**, through the following equation.

$$\mathbf{A} = \mathbf{UWV} \tag{1}$$

The diagonal elements of **W** are called singular values of **A** and are arranged in the order of magnitude. **U** and **V** are also rearranged consistently. The number of large singular values are equivalent to the number of species involved in the time-resolved spectra. For convenience, the qth column vector of **U** is represented by $\mathbf{u}_q(t)$, which has a dimension m and represents a temporal behavior of the qth mathematical species, and the qth row vector of **V** is represented by $\mathbf{v}_q(\nu)$, which has a dimension n and represents its spectral behavior. Note that the mathematical species are not equal to actual species. **U**, **V**, and **W** were numerically determined for a given data of **A**.

Model functions on temporal profiles of the population of a given species must be assumed to obtain practical meaning from this analysis. When there are k large values in **W**, the number of spectral species present is k. Accordingly, a temporal profile of population is assumed for each of the k species. If a population of pth species at delay time t is $\rho_p(t)$, the sum of $\rho_p(t)$ about p should be unity for any t and there would be k sets of $\rho_p(t)$, that is, $p = 1-k$. The SVD analysis identifies an appropriate set of coefficients r_{pq} ($p = 1-$k) which satisfy a given $\mathbf{u}_q(t)$.

$$\sum_p \rho_p(t) \mathrm{r}_{pq} = \mathbf{u}_q(t) \tag{2}$$

When there is no satisfactory set of r_{pq}, $\rho_p(t)$ should be reconstituted. When a set of r_{pq} is obtained for the qth vector, the same procedure is applied to the next q value. This procedure is used to determine all r_{pq} values for the k sets ($q = 1-k$). The spectrum of the pth species is given by $\sum_q r_{pq} w_q \mathbf{v}_q(\nu)$, in which w_q is the qth diagonal element of **W**.

Results

Figure 2 shows the ps-TR^3 spectra of NiOEP in pyridine in the time range −5 to 1000 ps, which were obtained by pumping

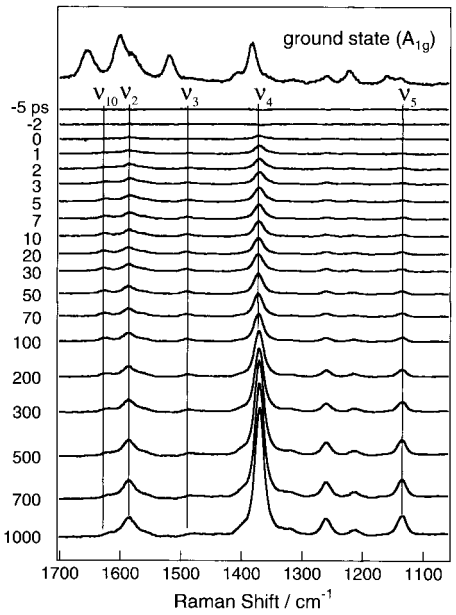

Figure 2. ps-TR^3 spectra of NiOEP in pyridine pumped at 516 nm and probed at 425 nm. The delay times are specified at the left side of each spectrum. The Raman spectra of solvent and four-coordinate ground-state NiOEP have been subtracted. The spectrum at the top depicts the probe-only spectrum of the ground-state NiOEP (solvent bands have been subtracted).

at 516 nm and probing at 425 nm. The static RR spectrum of ground-state NiOEP (probe-only spectrum) is depicted at the top. The contributions from pyridine and ground-state NiOEP have been subtracted already from the observed TR^3 spectra. In the 10 ps delay spectrum, bands are seen at 1627 (ν_{10}), 1587 (ν_2), 1491 (ν_3), 1372 (ν_4), 1135 (ν_5), and 667 (ν_7) cm^{-1}. These band positions are the same as those observed for the (d,d)-excited NiOEP in noncoordinating solvents such as toluene and THF.[9,13] (Note: ν_7 is not included in Figure 2). Therefore, it is evident that the metal (d,d)-excited state of NiOEP (B_{1g}) is formed within a few picoseconds. The initial asymmetric band shapes are gradually altered to more symmetric, and peak height becomes larger until ~50 ps.

A new set of Raman bands start to grow at 1586 (ν_2), 1370 (ν_4), 1260 (CH_2 twist), 1213 (ν_{13}), and 1135 (ν_5) cm^{-1} after ca. 100 ps of delay time and become noticeably intense around 1000 ps. Although these band center frequencies between 100 and 1000 ps are close to the frequencies observed at 10 ps, they are distinctly different. In addition, bands also appear at 1610 (ν_{10}) and 1484 (ν_3) cm^{-1} in this time frame. Therefore, it is apparent that population of a new species is increasing in the time range from 100 to 1000 ps. The frequencies of the RR bands of this species are closer to those of the B_{1g} species rather than those of the A_{1g} species in the spectrum shown at the top of Figure 2. The stretching frequencies of the porphyrin macrocycle above 1450 cm^{-1} mainly depend on the core size.[33] Since the electronic configuration of the metal is responsible for the core size, it is possible that the new set of bands arise from the metal excited B_{1g} species with different coordination numbers.

It is known that NiOEP adopts the six-coordinate structure, $B_{1g}(L)_2$ (L = piperidine), in piperidine with the absorption maximum at 419 nm due to the strong coordination ability of piperidine. Figure 3 compares the ps-TR^3 spectrum of NiOEP in pyridine at 1000 ps delay with the static ground-state RR spectrum of NiOEP in piperidine excited at 425 nm. It is evident that the two spectra are quite alike in terms of relative intensities and frequencies of bands. This indicates that the

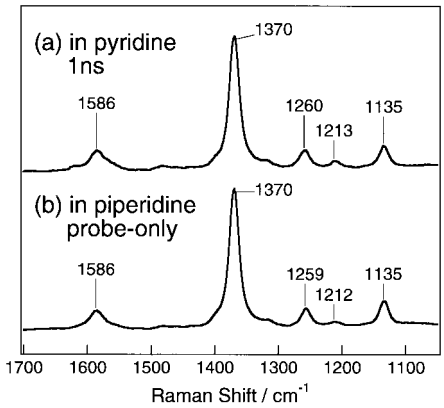

Figure 3. Comparison of the ps-TR^3 spectrum of NiOEP in pyridine at 1 ns delay (a) with the probe-only spectrum of NiOEP in piperidine (b). The spectra of solvent and the four-coordinate ground-state NiOEP have been subtracted. The probe wavelength is 425 nm.

TABLE 1: Observed Frequencies (cm^{-1}) of NiOEP in Various Solvents

		ν_{10}	ν_2	ν_3	ν_4	ν_5	ν_7	ref
pyridine	B_{1g}	1627	1587	1491	1372	1135	667	this work
	$B_{1g}(L)_2$		1586		1370	1135	667	this work
	A_{1g}	1657	1603	1521	1383	1137	668	this work
piperidine	$B_{1g}(L)_2$		1586		1370	1135	667	this work
THF	B_{1g}	1622	1584	1490	1372			9
	A_{1g}	1652	1601	1519	1382			9
toluene	B_{1g}	1629	1587	1494	1374			13
	A_{1g}	1657	1603	1520	1383			13

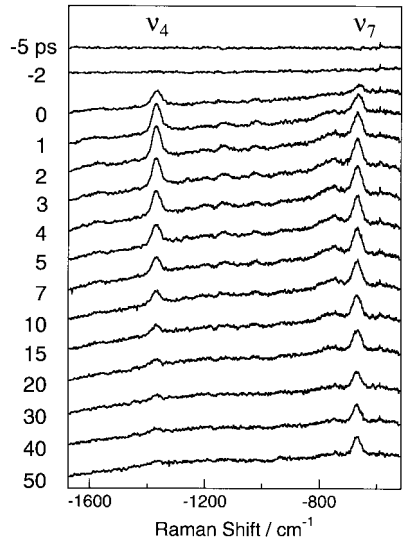

Figure 4. Anti-Stokes ps-TR^3 spectra of NiOEP in pyridine between −5 and +50 ps of delay time. Solvent- and probe-only spectra have been subtracted.

species generated at 1000 ps delay in pyridine is probably a six-coordinate species with two axially coordinated nitrogen ligands. The observed frequencies of the three species of NiOEP are summarized in Table 1.

Figure 4 shows the anti-Stokes ps-TR^3 spectra of NiOEP in pyridine in the delay time region between −5 and +50 ps. The ν_7 and ν_4 bands are clearly seen in the spectrum of 1 ps delay, but their intensities become weaker with increasing delay time. The Boltzman factors at 300 K for 667 (ν_7) and 1372 (ν_4) cm^{-1} are 0.041 and 0.0014, respectively. The ν_7 intensity at 50 ps delay may reflect the thermal population at the $v = 1$ level in the electronically excited (d,d) state. If ν_4 has a magnitude of Raman scattering cross-section similar to that of ν_7, its expected

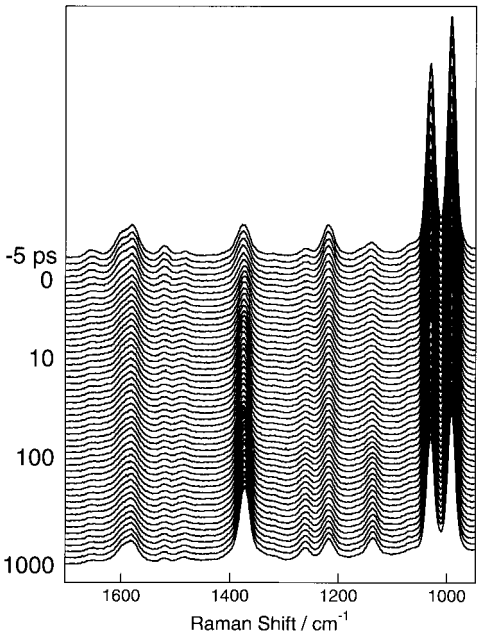

Figure 5. Fifty typical ps-TR^3 spectra of NiOEP in pyridine used for SVD analysis. Pump wavelength, 550 nm; probe wavelength, 415 nm.

intensity at the thermal equilibrium would be ca. 1/30th of that of ν_7. The disappearance of the ν_4 anti-Stokes band would thus be ascribed to vibrational relaxation. This indicates that the time constant of vibrational relaxation of NiOEP in pyridine is ca. 10 ps, which is similar to that in toluene.[13]

It is not known whether a five-coordinate species is formed during the process of conversion from the four-coordinate state at 10 ps delay to the six-coordinate state at 1000 ps delay, although no other species seems to appear in Figure 2. If a five-coordinate species was present transiently, it is possible that its RR bands would be less resonance enhanced because its absorption maximum is at a wavelength far from the maximum observed for the four- and six-coordinate species. To circumvent this potential problem, the ps-TR^3 spectra were measured with different probe wavelengths including 410, 415, and 425 nm at 0, 10, and 100 ps of delay time for the same pump wavelength. Nonetheless, no new bands were identified. Still, a small possibility that Raman bands of the putative five-coordinate species are severely overlapped with those of the four- or six-coordinate species cannot be ruled out completely. Therefore, the SVD analysis was carried out for ps-TR^3 data to search for the putative five-coordinate species.

Since a high-quality SVD analysis requires an increased number of data points, we measured the TR^3 spectra pumped at 550 nm and probed at 415 nm for 99 different delay times (only 50 spectra are shown in Figure 5). The results of SVD analysis for these data are illustrated in Figure 6. The distribution of 10 large values of w_q's are plotted in panel a, where open circles denote the plots against the ordinate scale expanded by 20 times. Since the values are definitely smaller for w_q's below the sixth, we judged that there were five species involved in TR^3 spectra shown in Figure 5. The five $\mathbf{u}_q(t)$ vectors corresponding to five large w_q are depicted by the lower five traces in panel b, while upper traces represent the remaining four $\mathbf{u}_q(t)$'s. The zero point for each plot is vertically shifted to avoid overlapping, but the their ordinate scales are in common. It is noted that one of $\mathbf{u}_q(t)$'s strongly reflects a species involving immediate rise and rapid decay (the decay constant is ca. 10 ps), suggesting the presence of a vibrationally excited species among the five. The lower five traces in panel

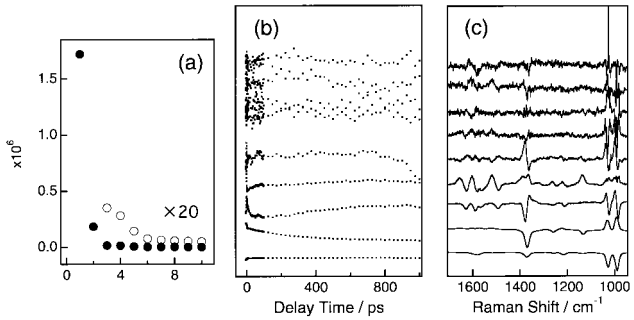

Figure 6. Results of SVD analysis: (a) 10 largest singular values w_q; (b) $\mathbf{u}_q(t)$ vectors (temporal components) for the 10 largest w_q values; (c) $\mathbf{v}_q(\nu)$ vectors (spectral components) for the 10 largest w_q values. The $\mathbf{u}_q(t)$ and $\mathbf{v}_q(\nu)$ are arranged from the bottom in the order of magnitude of the corresponding w_q. The scales of the ordinate are in common for the 10 curves, but the origin is vertically shifted for improved visualization.

c represent $\mathbf{v}_q(\nu)$'s of the species corresponding to five large w_q's, while others show those of the remaining four.

The five spectral species involved were identified to be (1) a four-coordinate ground-state species (A_{1g}), (2) a vibrationally excited and electronically (d,d) excited four-coordinate species (B_{1g}*), (3) a thermally equilibrated but electronically (d,d) excited four-coordinate species (B_{1g}), (4) a thermally equilibrated but electronically excited six-coordinate species ($B_{1g}(L)_2$), and (5) solvent molecules affected by transient absorption changes. The model functions of the five species were constructed on the basis of Scheme 1. The NiOEP photoexcited to (π,π*) in pyridine, denoted as E_u, is converted to the B_{1g}* state within a subpicosecond. Since the formation of the four-coordinate B_{1g}* species occurs within the present time resolution, we start from this species. For simplicity, the "B_{1g}*", "B_{1g}", "$B_{1g}(L)_2$", and "A_{1g}" species are represented as A, B, C, and D, respectively, in the following rate equations:

$$\mathrm{d[A]}/\mathrm{d}t = -k_1[\mathrm{A}] \tag{3A}$$

$$\mathrm{d[B]}/\mathrm{d}t = k_1[\mathrm{A}] - (k_2 + k_3)[\mathrm{B}] \tag{3B}$$

$$\mathrm{d[C]}/\mathrm{d}t = k_2[\mathrm{B}] \tag{3C}$$

$$\mathrm{d[D]}/\mathrm{d}t = k_3[\mathrm{B}] \tag{3D}$$

where k_2 is regarded as a pseudo-first-order rate constant involving the concentration of coordinating ligands, although the true rate constant has the dimension of $s^{-1}M^{-1}$. The analytical solutions for the differential equations above are as follows:

$$[\mathrm{A}] = [\mathrm{A}]_0 \mathrm{e}^{-k_1 t} \tag{4A}$$

$$[\mathrm{B}] = \frac{k_1[\mathrm{A}]_0}{(k_2 + k_3) - k_1}(\mathrm{e}^{-k_1 t} - \mathrm{e}^{-(k_2+k_3)t}) \tag{4B}$$

$$[\mathrm{C}] = \frac{k_1 k_2[\mathrm{A}]_0}{(k_2 + k_3) - k_1}\left\{\frac{1}{k_1}(1 - \mathrm{e}^{-k_1 t}) - \frac{1}{k_2 + k_3}(1 - \mathrm{e}^{-(k_2+k_3)t})\right\} \tag{4C}$$

$$[\mathrm{D}] = \frac{k_1 k_3[\mathrm{A}]_0}{(k_2 + k_3) - k_1}\left\{\frac{1}{k_1}(1 - \mathrm{e}^{-k_1 t}) - \frac{1}{k_2 + k_3}(1 - \mathrm{e}^{-(k_2+k_3)t})\right\} \tag{4D}$$

SCHEME 1: Scheme for Construction of Model Functions on SVD Analysis

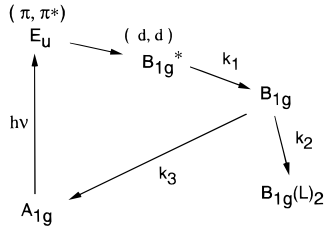

Here, $[A]_0$ represents the initial concentration of A (=photoexcited fraction) and $\sum\rho_p = 1$ is kept for $p = 1-4$ (ρ_p is $[X]/[A]_0$ and X is A−D). The fifth component arises from the intensity changes of strong solvent bands around 1000 cm^{-1}, and its model function reflects the transient absorption changes of the sample solution at wavelengths corresponding to ∼1000 cm^{-1} of Raman shift.

The model functions for populational changes of the five species are displayed in Figure 7, where the populations of the B_{1g}* (a), B_{1g} (b), $B_{1g}(L)_2$ (c), and A_{1g} species (d) are plotted against delay time. The model function of self-absorption effects is also delineated by Figure 7e. With these functions, we obtained r_{pq} which can reproduce the five $\mathbf{u}_q(t)$ curves shown in Figure 6b. After some adjustments of parameters by trial and error for satisfactory reproduction of $\mathbf{u}_q(t)$, the first-order or pseudo-first-order rate constants were finally determined to be $k_1 = 1.0 \times 10^{11}$ s^{-1}, $k_2 = 5.2 \times 10^8$ s^{-1}, and $k_3 = 1.5 \times 10^9$ s^{-1}. These values, corresponding to the time constants of 10, 1900, and 670 ps, respectively, were used in the construction of the model functions shown in Figure 6.

The practical spectra of the five assumed species were calculated by using w_q, r_{pq}, and $\mathbf{v}_q(\nu)$. The results are depicted in Figure 8, where peaks marked by an asterisk denote the solvent bands. First, spectrum d is assigned to the A_{1g} species, because the peak frequencies and spectral pattern are very close to the probe-only spectrum shown in Figure 2. Spectrum c is assigned to the $B_{1g}(L)_2$ species from its similarity to the spectrum

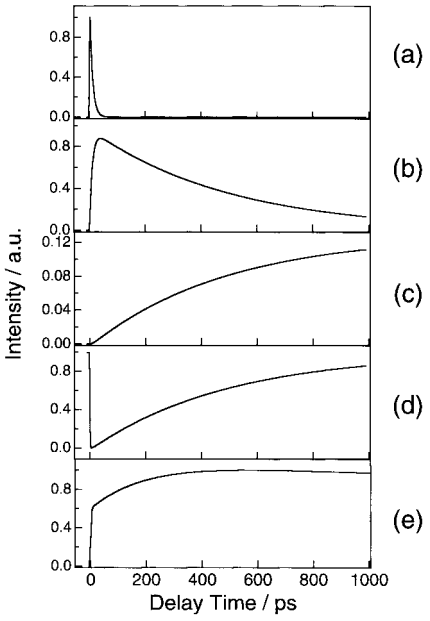

Figure 7. Model functions of temporal profiles of the five species. a−d reflect the relative population of A through D, respectively, calculated on the basis of Scheme 1. $\sum\rho_p(t) = 1$ is satisfied for any t. The ordinate scale of function e is arbitrary, while this reflects the change of self-absorption effects of NiOEP.

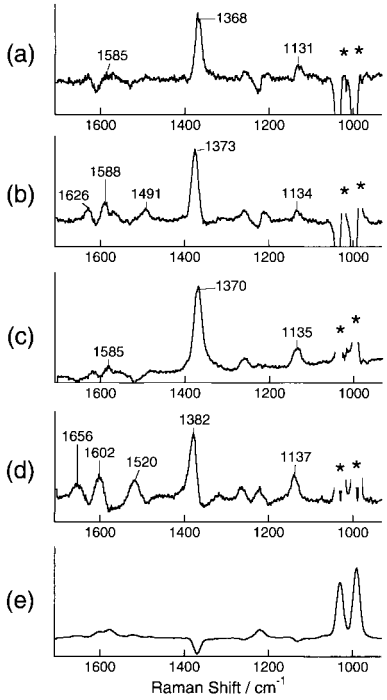

Figure 8. Reconstructed spectra of the five plausible species obtained with the spectral components of SVD analysis and model functions shown in Figure 6: (a) the B_{1g}* species; (b) the B_{1g} species; (c) the $B_{1g}(L)_2$ species; (d) the A_{1g} species; (e) self-absorption effect.

at 1000 ps delay. Spectrum b is assigned to the B_{1g} species, since its spectrum is close to the transient spectra of NiOEP in toluene solution observed around 20−50 ps of delay time. Spectrum a is presumably assignable to the B_{1g}* species, because the frequencies of all bands are slightly lower than the corresponding bands of spectrum b, (to be discussed later). Spectrum e reflects the effective spectrum of solvent molecules influenced by the temporal changes of absorption intensity of the solution around the probed wavelength region. Thus, the observed ps-TR[3] spectra could be interpreted successfully with Scheme 1. This means that the five-coordinate species, if present, is not populated enough to be detected by the present Raman experiments.

The lack of evidence for the existence of the five-coordinate species implies that it may be too unstable to exist under these conditions. To confirm this property, the steady-state absorption spectra of NiOEP in the ground electronic state were examined. It is known that NiOEP in the ground state forms mainly a six-coordinate complex in piperidine and a four-coordinate complex in toluene. Spectral changes upon mixing of these two equiconcentration solutions are shown in Figure 9. It is apparent that visible absorption spectra change with isosbestic points. The putative five-coordinate species would be expected to exhibit an absorption spectrum distinctly different from the spectra of the four- and six-coordinate species. If such a five-coordinate species existed, there should be no isosbestic points in the series of spectra. The results shown in Figure 9 mean that only two components, the four- and six-coordinate complexes, are in equilibrium within the toluene−piperidine mixed solutions. Therefore, there is no five-coordinate species in a stationary state of the ground-state NiOEP, and it is probable that the same character might be retained by the photoexcited species.

Discussion

Species Present in the Initial Stage of Photoexcitation. One may argue that the initial stage of photoexcitation of NiOEP

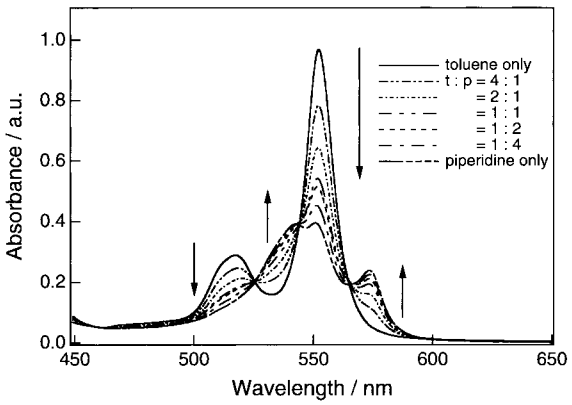

Figure 9. Steady-state absorption spectra of NiOEP in mixed solvents of toluene and piperidine.

involves conformational relaxation of the porphyrin macrocycle in addition to vibrational relaxation. In fact, for NiOEP in toluene, two ν_{10} bands were observed at 1616 and 1625 cm^{-1} in the delay time region between 3 and 10 ps, but the former and latter became weaker and stronger, respectively, with increasing delay time.[13] This was attributed to a conformational change of the macrocycle. At the initial stage of photoexcitation, the planar and ruffled forms of the porphyrin coexist in the ground state, but in the (d,d) excited state with an electron in the $d_{x^2-y^2}$ orbital, the planar form is more stabilized due to better matching of the ionic radius to the core size of the macrocycle.[11]

If a similar phenomenon took place for NiOEP in pyridine, spectrum a in Figure 8 might be assigned to the conformationally unrelaxed B_{1g} species rather than to the vibrationally excited B_{1g} species. The presence of such a nonplanar form may not be ruled out, but the assignment of spectrum a to the nonplanar species is less likely for the following reasons: First, the splitting of the ν_{10} is not observed in the initial stage of ps-TR^3 spectra shown in Figure 4. Second, it is known that even a small deviation of the macrocycle from planarity causes a considerable downshift of the ν_{10} frequency.[34] The ν_{10} frequency in spectrum a is not downshifted. Its frequency is 1626 cm^{-1}, the same frequency observed in spectrum b, (although a trough is seen around 1600 cm^{-1} owing to the presence of a strong solvent band). Third, the ν_4 frequency in spectrum a is definitely shifted from that of spectrum b, while the ν_4 frequency is insensitive to nonplanarity.[19a]

On the other hand, all bands are slightly shifted to lower frequencies in spectrum a compared with those in spectrum b, while their spectral patterns are alike. This phenomenon is observed for vibrationally excited species when vibrational anharmonicity is present. Furthermore, the decay constant of the B_{1g}* species is close to the decay constant of the anti-Stokes Raman bands shown in Figure 4. One may expect that vibrationally excited species should give rise to asymmetric band shape broader on the low-frequency side. This would be true for molecules in a thermal equilibrium, but note that spectrum a is obtained from SVD analysis for a pure vibrationally excited species ($v \geq 1$).

Kinetics in Photoexcited States. Application of SVD analysis to a series of ps-TR^3 spectra has enabled us to determine the number of species involved and also the rate constants of the reactions shown in Scheme 1. Kim et al.[4] previously studied the transient absorption spectra and determined the time constant for the decay of the B_{1g} species to be 450 ps. This value involves the reactions for two pathways: $B_{1g} \rightarrow A_{1g}$ and $B_{1g} \rightarrow B_{1g}(L)_2$ with rate constants of 670 and 1900 ps, respectively. The two kinds of measurements are in qualitative agreement that the overall decay of the B_{1g} species appears slightly faster than the rate of a single reaction of $B_{1g} \rightarrow A_{1g}$. In the transient absorption study, however, the absorption band is very broad and bands of several species are overlapped in many cases. Each species is more easily identified in the TR^3 spectra than in the absorption spectra. TR^3 spectroscopy is thus better suited for studies of reaction dynamics of metal porphyrin systems.

The time constant for the coordination of pyridine to NiOEP (1900 ps) is longer than those for other bimolecular reactions by 1 or 2 orders of magnitudes. For example, the time constants for geminate recombination of NO and O_2 to Fe of myoglobins are on the order of several picoseconds.[35,36] In the photodissociation of $M(CO)_6$ (M = Cr, Mo, or W), subsequent binding of a solvent molecule (alcohol) to a photodissociated fragment, $M(CO)_5$, is noted to take place within several picoseconds.[37,38] It has been reported from transient IR studies of reactions between photofragments and solvents[39,40] that the time constants for the formation of HCN and ClCN upon photolysis of ICN in chloroform are 194 and 140 ps, respectively.[39] These results suggest that bimolecular reactions can occur in subnanosecond time regime when reacting molecules are present in close proximity.

Coordination of a single solvent molecule to NiOEP may take place within this time frame. The acceptance angle for coordination of pyridine to the Ni(II) ion of NiOEP is limited. In solution, however, the rotational diffusion for pyridine is fast, as the reorientational relaxation time of pyridine is reported to be approximately 5 ps.[41] The coordination of a single solvent molecule to NiOEP may take place in this time frame, yielding the five coordinate species, $B_{1g}(L)$. Because the $B_{1g}(L)$ species was not identified in the course of conversion to the $B_{1g}(L)_2$ species, there are two possibilities about the kinetics of the formation of the $B_{1g}(L)_2$ species via the $B_{1g}(L)$ species: (1) coordination of a single pyridine molecule induces higher affinity of the Ni(II) ion for the second pyridine ligand (i.e. $B_{1g}(L)$ formation is rate-limiting), and (2) most of the $B_{1g}(L)$ species immediately decomposes into the B_{1g} NiOEP and L, leaving only a small fraction of the $B_{1g}(L)$ species to form the $B_{1g}(L)_2$ species with another pyridine molecule locating in the proximity with proper orientation (i.e. $B_{1g}(L)_2$ formation is rate-limiting). The rotational motion of pyridine molecules on the time scale of 10 ps suggests that the latter case is more probable. The $B_{1g}(L)_2$ formation limiting process might be explained by the concerted collision of two pyridine molecules with NiOEP, and its probability would be ca. 10^3 times less likely than the coordination of a single pyridine molecule to NiOEP. Therefore, the formation of the six-coordinate complex from the five-coordinate species is the rate-determining step, and the observed value reflects this process.

The question arises as to why the five-coordinate complex is unstable compared with the six- and four-coordinate complexes. A qualitative view from a simple MO description suggests a following scheme: When the d_{z^2} orbital of Ni(II) containing one electron overlaps with the lone pair orbital of one pyridine, the mixing results in bonding and antibonding orbitals. The bonding orbital is doubly occupied, and the antibonding is singly occupied. On the other hand, when two pyridines interact with the d_{z^2} orbital, one more bonding orbital doubly occupied would be formed, while the antibonding orbital is singly occupied. The amount of stabilization contributed by the additional MO for the six-coordinate complex depends on the energy level of the lone pair orbital of pyridine relative to the d_{z^2} orbital of Ni(II). Whatever the case, coordination of two pyridine ligands is more

energetically favorable than ligation of a single pyridine. This assumes that the porphyrin conformations of the six- and five-coordinate complexes are alike. Actually, however, the six-coordinate complex is planar, but the five-coordinate complex is expected to be domed, and accordingly energy levels of MO's other than the metal d_{z^2} would also be different between the two structures. Explanations for the instability of the five-coordinate complex should take such conformational changes into account.

In conclusion, the ps-TR^3 experiments on NiOEP in pyridine demonstrate the coordination of pyridine in the metal (d,d) excited state. SVD analysis of the ps-TR^3 data indicates the presence of four different NiOEP species, as shown in reaction Scheme 1, and has also allowed us to determine the rate constants for individual processes. This indicates the concerted coordination of two pyridine molecules to the axial positions of the (d,d)-excited NiOEP.

Acknowledgment. The authors thank Dr. Mark Roach of this institute for helpful discussion. This study was supported by a Grant-in-Aid for Scientific Research on Priority Areas (Molecular Biometallics) from the Ministry of Education, Science, Sports, and Culture, Japan to T.K. (Grant 08249106).

References and Notes

(1) Ake, R. L.; Gouterman, M. *Theor. Chim. Acta* **1970**, *17*, 408.
(2) Kobayashi, T.; Straub, K. D.; Rentzepis, P. M. *Photochem. Photobiol*. **1979**, *29*, 925.
(3) Chirvony, V. S.; Dzhagarov, B. M.; Timinskii, Yu. V.; Gurinovich, G. P. *Chem. Phys. Lett*. **1980**, *70*, 79.
(4) Kim, D.; Kirmaier, C.; Holten, D. *Chem. Phys*. **1983**, *75*, 305.
(5) Rodriguez, J.; Holten, D. *J. Chem. Phys*. **1989**, *91*, 3525.
(6) Rodriguez, J.; Kirmaier, C.; Holten, D. *J. Chem. Phys*. **1991**, *94*, 6020.
(7) Chikishev, A. Yu.; Kamalov, V. F.; Koroteev, N. I.; Kvach, V. V.; Shkurinov, A. P.; Toleutaev, B. N. *Chem. Phys. Lett*. **1988**, *144*, 90.
(8) (a) Courtney, S. H.; Jedju, T. M.; Friedman, J. M.; Alden, R. G.; Ondrias, M. R. *Chem. Phys. Lett*. **1989**, *164*, 39. (b) Courtney, S. H.; Jedju, T. M.; Friedman, J. M.; Rothberg, L.; Alden, R. G.; Park, M. S.; Ondrias, M. R. *J. Opt. Soc. Am*. **1990**, *B7*, 1610.
(9) Sato, S.; Kitagawa, T. *Appl. Phys*. **1994**, *B59*, 415.
(10) (a) Findsen, E. S.; Shelnutt, J. A.; Friedman, J. M.; Ondrias, M. R. *Chem. Phys. Lett*. **1986**, *126*, 465. (b) Findsen, E. W.; Shelnutt, J. A.; Ondrias, M. R. *J. Phys. Chem*. **1988**, *92*, 307.
(11) Apanasevich, P. A.; Kvach, V. V.; Orlovich, V. A. *J. Raman Spectrosc*. **1989**, *20*, 125.
(12) Kruglik, S. G.; Apanasevich, P. A.; Kvach, V. V.; Orlovich, V. A. *Laser Applications in Life Sciences*. *Proceedings of SPIE*; International Society for Optical Engineering: Bellingham, WA, 1994; Vol. 2370, p 196.
(13) Kruglik, S. G.; Mizutani, Y.; Kitagawa, T. *Chem. Phys. Lett*. **1997**, *266*, 283.
(14) Eom, H. S.; Jeoung, S. C.; Kim, D.; Ha, J.-H.; Kim, Y. R. *J. Phys. Chem*. **1997**, *101A*, 3661.
(15) Cullen, D. L.; Meyer, E. F., Jr. *J. Am. Chem. Soc*. **1974**, *96*, 2095.
(16) Brennan, T. D.; Scheidt, W. R.; Shelnutt, J. A. *J. Am. Chem. Soc*. **1988**, *110*, 3919.
(17) (a) Kitagawa, T.; Abe, M.; Ogoshi, H. *J. Chem. Phys*. **1978**, *69*, 4516. (b) Abe, M.; Kitagawa, T.; Kyogoku, Y. *J. Chem. Phys*. **1978**, *69*, 4526.
(18) Li, X.-Y.; Czernuszewicz, R. S.; Kincaid, J. R.; Stein, P.; Spiro, T. G. *J. Phys. Chem*. **1990**, *94*, 47.
(19) (a) Alden, R. G.; Crawford, B. A.; Doolen, R.; Ondrias, M. R.; Shelnutt, J. A. *J. Am. Chem. Soc*. **1989**, *111*, 2070. (b) Jentzen, W.; Unger, E.; Karvounis, G.; Shelnutt, J. A.; Dreybrodt, W.; Schweitzer-Stenner, R. *J. Phys. Chem*. **1996**, *100*, 14184.
(20) Czernuszewicz, R. S.; Li, X.-Y.; Spiro, T. G. *J. Am. Chem. Soc*. **1989**, *111*, 7024.
(21) Kim, D.; Oliver, Y.; Spiro, T. G. *Inorg. Chem*. **1986**, *25*, 3988.
(22) Uesugi; Y.; Mizutani; Y.; Kitagawa, T. *Rev. Sci. Instrum*. **1997**, *68*, 4001.
(23) Zimanyi, L.; Lanyi, J. K. *Biophys. J*. **1993**, *64*, 240.
(24) Thorgeirsson, T. E.; Milder, S. J.; Miercke, L. J. W.; Betlach, M. C.; Shand, R. F.; Stroud, R. M.; Kliger, D. S. *Biochemistry* **1991**, *30*, 9133.
(25) Chen, W.-G.; Braiman, M. S. *Photochem. Photobiol*. **1991**, *54*, 905.
(26) Hofrichter, J.; Henry, E. R.; Lozier, R. H. *Biophys. J*. **1989**, *56*, 693.
(27) Yuzawa, T.; Hamaguchi, H. *J. Mol. Struct*. **1995**, *352/353*, 489.
(28) Ansari, A.; Jones, C. M.; Henry, E. R.; Hofrichter, J.; Eaton, W. A. *Biophys. J*. **1993**, *64*, 852.
(29) Lambright, D. G.; Balasubramanian, S.; Boxer, S. G. *Biochemistry* **1993**, *32*, 10116.
(30) Hug, S. J.; Lewis, J. W.; Einterz, C. M.; Thorgeisson, T. E.; Kliger, D. S. *Biochemistry* **1990**, *29*, 1475.
(31) Hofrichter, J.; Henry, E. R.; Sommer, J. H.; Deutsh, R.; Ikeda-Saito, M.; Yonetani, T.; Eaton, W. A. *Biochemistry* **1985**, *24*, 2667.
(32) Press: W. H.; Flannery, B. P.; Teukolsky, S. A.; Vetterling, W. T. *Numerical Recipes in C*; Cambridge University Press: Cambridge, U.K., 1988; p 60.
(33) Spaulding, L. D.; Chang, C. C.; Yu, N.-T., Felton, R. H. *J. Am. Chem. Soc*. **1975**, *97*, 2517.
(34) Prendergast, K.; Spiro, T. G. *J. Am. Chem. Soc*. **1992**, *114*, 3793.
(35) Duprat, A. F.; Traylor, T. G.; Wu, G.-Z.; Colotta, M.; Sharma, V. S.; Walda, K. N.; Magde, D. *Biochemistry* **1995**, *34*, 2634.
(36) Gibson, Q. H.; Regan, R.; Elber, R.; Olson, J. S.; Carver, T. E. *J. Biol. Chem*. **1992**, *267*, 22022.
(37) Joly, A. G.; Nelson, K. A. *J. Phys. Chem*. **1989**, *93*, 2876.
(38) Joly, A. G.; Nelson, K. A. *Chem. Phys*. **1991**, *152*, 69.
(39) Raftery, D.; Gooding, E.; Romanovsky, A.; Hochstrasser, R. M. *J. Chem. Phys*. **1994**, *101*, 8572.
(40) Raftery, D.; Iannone, M.; Phillips, C. M.; Hochstrasser, R. M. *Chem. Phys. Lett*. **1993**, *201*, 513.
(41) Ito, N.; Kato, T. *J. Phys. Chem*. **1984**, *88*, 801.